arXiv:1605.07257v1 [quant-ph] 24 May 2016

Characterizing micro-macro transitions with slow light

Zhifan Zhou[1,†,⋆], Ulrich Vogl[2], Ryan T. Glasser[3], Zhongzhong Qin[1], Yami Fang[1], Jietai Jing[1,†], Weiping Zhang[1,†]

[1] *Quantum Institute for Light and Atoms, State Key Laboratory of Precision Spectroscopy, Department of Physics, East China Normal University, Shanghai 200062, P. R. China*

[2] *Max Planck Institute for the Science of Light, Günther-Scharowsky-Strasse 1, Bau 24, 91058 Erlangen, Germany*

[3] *Department of Physics and Engineering Physics, Tulane University, 6400 Freret Street, New Orleans, Louisiana 70118, USA*

Abstract

The transition between the microscopic to the macroscopic world is of broad fundamental and technological significance. Optical parametric amplifiers allow for amplifying single photons to the macroscopic level, but the underlying temporal dynamics are still not well understood. Slow light, in which the group velocity is delayed via quantum interference, is an effective tool to interrogate the temporal dynamics of light-matter interactions. Here, we demonstrate a scheme to characterize micro-macro transitions with slow light based on a four-wave mixing linear amplification process in a hot rubidium vapour. The scheme exhibits strong dispersion which is sensitive to the input's change at the single-photon level, resulting in a nonlinear decay of the micro-macro transition time with the increased microscopic input. The present system is suitable for the study of the relevant time scale of quantum-to-classical transitions and the potential impact from fundamental effects such as gravity, as indicated by recent proposals.

† Corresponding authors, emails: zfzhoucom@gmail.com(Z.Z.), jtjing@phy.ecnu.edu.cn(J.J.), wpzhang@phy.ecnu.edu.cn(W.Z.). ⋆ Current affiliations: *Department of Physics, Ben-Gurion University of the Negev, Beersheba 84105, Israel.* (Z.Z.)

The dynamics of micro-macro transitions is instrumental to understanding the process of quantum-to-classical transitions [1–15]. Photons are promising candidates for this investigation due to the efficient light-matter interactions that have been achieved [4–18], and their inherent bosonic nature which in principle allows for unlimited occupations in the same quantum state. The connection between micro-to-macro transitions and quantum-to-classical transitions has been investigated with optical parametric amplifiers based on crystal-systems [8] and with four-wave mixing in fiber-systems [15]. However, due to the large inhomogeneous broadening in the noted condensed-matter materials, the dispersion property and the observed micro-to-macro transition times are usually not sensitive to the microscopic input's change at the single-photon-level [5–8, 15].

Alkali-metal atomic vapour, with high optical depths and much smaller inhomogeneous broadening, allows for quantum interference between different channels, e.g. electromagnetically induced transparency (EIT) [19–21]. EIT based on quantum interference can render an otherwise opaque medium transparent over a narrow spectral range. The resulting steep dispersion and delayed group-velocity are used to buffer optical information and interrogate the dynamics of the light-matter interaction [22–26]. The group-velocity delay of single-photon-level states has been demonstrated at the level of micro-micro transitions without amplification [27–29]. Recent proposals also pointed out that under the presence of a gravitational field, the spatially-varying deflection of slow light propagation is anticipated to be accessible [30, 31], which offers the possibility to study photons' quantum behavior in a gravitational background [32, 33].

To show the micro-macro transitions associated with slow light, efficient amplification for input single-photon-level pulses is required. The four-wave mixing (FWM) process based on the double-lambda configuration (Fig.1b) in hot rubidium vapour [34] has provided a powerful tool for this purpose. In this process, two pump photons are converted into one probe photon and one conjugate photon in each cycle such that the atomic states are preserved after each cycle. The light fields can be coupled via the atomic coherence between the two hyperfine ground states, which allows for reducing resonant losses and increasing the relevant nonlinearities [21, 23, 26]. Combined with the large detuning, resonant absorption and spontaneous emission are suppressed. With a strong pump light beam, which ensures the condition of low pump depletion, the system behaves like a linear optical amplifier (LOA) for the probe and the conjugate. Furthermore, the quantum interference via the coupling

between the light fields and the atomic coherence result in a large group-velocity delay [24, 25, 35]. Here, we make use of the FWM-based LOA and a significant slow light effect to probe the micro-macro transition's temporal dynamics, involving a large dynamic range of 70 dB in photon flux. The results reveal that despite linear amplification for different inputs at the single-photon level, the observed group-velocity delay used for characterizing the micro-macro transitions decays nonlinearly with an increased input average number of photons.

Results

Micro-macro transitions A high-gain FWM-based LOA requires a high effective optical depth, such that a 75-mm-long rubidium cell (Fig.1) with a high atomic density (2×10^{13} atoms/cm^3) at a temperature of 130°C is used. We begin by characterizing the FWM-based amplification process by seeding a bright coherent beam (27 μW) at the near-resonance probe frequency and measuring the output's dependence on the pump power. The gain is measured as the ratio between the output conjugate power and the input seed in the probe mode. The gain of FWM, $G = e^{-g \cdot L}$, where g is the gain coefficient and L is the length of the rubidium cell, is found to exponentially increase with the pump power (Fig.2a). Correspondingly, the gain coefficient is then found to be linearly decreasing with pump power (Fig.2b). At a pump power of 130mW, the gain coefficient is 0, which indicates that the gain is unity. The gain coefficient keeps decreasing linearly until saturation around 180 mW. It is worth noting that the gain for a low-light-level seed may be much higher than a high-light-level seeds gain (for example, 27 μW here) in the amplification process [36], due to the limited pump power and saturation of the gain medium.

We operate here in the high-gain regime to demonstrate the LOA for the single-photon-level input with a pump power of 300 mW, as the gain-saturated pump power is higher for the low-light-level input. When the input probe and conjugate modes are vacua, the strong coupling between the pump field and the atoms in FWM can provide large gain for the spontaneously emitted probe and conjugate photons in a single-pass configuration. Conical emission is then generated with an output pattern of a ring with the photons at the probe and conjugate frequencies [37, 38]. The angle between the pump beam and the ring is 8 mrad, indicating the optimal orientation to fulfill the phase-matching condition in this FWM scheme [39]. As the gain is high, a single-photon-level injected probe field along the

azimuthal angle can trigger the stimulated FWM process, amplifying the input probe and generating the conjugate [37].

According to Fig.1b, the probe photons are more near-resonant than the conjugate photons, and are used to seed the process. By injecting a weak probe beam, stimulated FWM occurs in which the probe is amplified by a factor of 10^7 and a conjugate is generated on the opposite side of the pump (Fig.1c). We investigate the output power of the conjugate, which suffers less from the Doppler-broadened absorption, as a function of averaged input probe photon number from 1 to 10 photons (Fig.2c) and for a large scale (Fig.2d), showing the linear amplifications for a large dynamical range for the low-light-level input. As the outputs are at the macroscopic level, the output signals are detected by off-the-shelf linear detectors (non-single-photon counting detectors). The results demonstrate that the LOA is capable of operating at the single-photon level and the linearity is preserved well up to ∼1000 input averaged number of photons. The signals observed on the oscilloscope are averaged for 10,000 times for the lowest plot in Fig.2c and 1,000 times for the highest plot in Fig.2c in order to achieve a high signal to noise ratio (SNR).

Gain profile and slow light In order to characterize the dispersion properties of the FWM process, the probe frequency is scanned across the two-photon resonance (with the pump shown in Fig.1b), revealing two nearly Lorentzian gain profiles at the probe and conjugate frequencies with full width half maximum (FWHM) linewidths of 1.48 MHz and 1.53 MHz, respectively, as shown in Fig.3a and Fig.3b. Both of the two gain profiles are much narrower than the natural linewidth of Rb^{85}, 5.75 MHz, due to the quantum interference based on the atomic coherence in the double-lambda configuration [24, 25, 40]. The amplitude of the output probe mode is smaller than that of the conjugate mode due to the additional Doppler-broadened absorption at the probe frequency.

The steep dispersions resulting from the narrow gain profiles give rise to the slow group velocities for the output probe and conjugate signals [21, 27–29, 43], when tuned to the gain-line center. In Fig.3c, the generated group-velocity delays are displayed with the injected probe pulse containing 0.7 photons on average. The reference pulse is obtained by measuring the injected strong probe pulses without attenuation when the pump beam is blocked and the probe's frequency is tuned far away from the atomic resonances. The group-velocity delays of the probe and conjugate pulses are 672 ns and 592 ns, with fractional delay of 1.14

and 1.01, respectively (Fig.3c). One noted feature is that the conjugate pulse is faster than the probe pulse, which is a well-understood property of the dynamics of the FWM process based on double-lambda configuration [24, 25, 40].

Dispersion-delay time matching The strong coupling at the low-light-level injection allows for investigating the dependence of the dispersion relation and the group velocity delay on the averaged photon number of the input light, which is shown in Fig.4. Due to the strong nonlinear coupling, the stronger input continuous power will make the bandwidths of the gain profiles broader (Fig.4a and Fig.4c). To describe this effect, we utilize the Raman gain model based on atomic coherence [40–42]:

$$\Gamma_{gain} = \frac{\eta \cdot \Omega_{pump} \cdot \Omega_{probe}}{\Delta_{Raman}}, \tag{1}$$

involving the gain profile′s bandwidth, Γ_{gain}, the Rabi frequencies of pump and probe, Ω_{pump} and Ω_{probe}, and the coupling strength, η, which is related with the amplification. The broadening of the gain profile will lead to less steep dispersion and result in a shorter group velocity delay of the pulses [41, 43], which is characterized as $\tau_d = 1/\Gamma_{gain}$ [40, 41].

Here we are interested in characterizing the relationship between the dispersion and the resulting delay time in the linear amplification regime indicated in Fig.2(d). The results of the gain bandwidth when the input continuous probe power increases from 0.5pW to 400pW are shown in Fig.4a and Fig.4c for the probe and conjugate, respectively. With the pulse lengths of 587ns, that power range corresponds to the range for the input averaged photon number from 1 to 800 in Fig.4b and Fig.4d, well within the linear amplification regime. The resulting change in bandwidth and delay time agree quantitatively with Eq.(1) over a large dynamic range.

The typical delayed pulses in the conjugate mode for different averaged input photon numbers are shown in Fig.4e. While increasing the input power causes other nonlinearities [44] which are responsible for the slight pulse distortions, the pulse peaks (Fig.4f) follow varied delay times depending on the the averaged input photon numbers as predicted by Eq.(1). The pulses shown in Fig.4f have the background subtracted and are normalized to assist in the visualization.

Discussion

We have demonstrated a high-gain linear optical amplifier converting the microscopic level input into the macroscopic level output based on the four-wave mixing process in hot rubidium vapour. Despite the gains for different inputs at the single-photon-level being identical, the temporal dynamics for each micro-macro transition are resolved in this highly dispersive medium, showing the decay of the group-velocity delay with the input averaged number of photons. The experiment has shown good dispersion-delay time matching in a large dynamic regime. As the scheme can be readily extended to generate quantum states both at microscopic and macroscopic level [34, 35, 45], this demonstration will be useful for investigating the time scale for the quantum-to-classical transition and the amplification process of entangled states [5–9, 11, 12, 15] in a highly dispersive medium.

It has been pointed out recently [30, 31] that slow light propagation in the presence of a gravitational field may allow for gravitational deflections that are on a laboratory-length scale. We anticipate that this deflection may have an effect on the micro-to-macro transition's temporal dynamics, in which the results described here should allow for interrogating such fundamental behavior. The ability to observe slow-light effects within a micro-to-macro transition, and the potential quantum-to-classical transition, will offer an efficient platform to study the fundamental principles involved in the overlap between quantum mechanics and general relativity such as gravitational induced decoherence and wave function collapse mechanisms [32, 33, 46, 47].

Methods Summary

The laser beams used in the experiment are derived from a Ti:Sapphire laser (Matisse, Spectra-Physics) blue-detuned roughly 1.25 GHz from the $5S_{1/2}$ (F=2) to $5P_{1/2}$ transition in ^{85}Rb. The pump is linearly polarized and is spatially filtered using a single-mode optical fiber. The injected probe is derived from one part of the pump and down-shifted by approximately 3.036 GHz by double-passing an acoustic-optical modulator. Afterwards the probe is spatially filtered using another single-mode optical fiber. The pump and probe beams are perpendicularly polarized and combined on a Glan-Taylor polarizer that has an extinction ratio of 10^5:1. A naturally abundant rubidium vapour cell with a length of 7.5 cm is heated to 130°C as the working temperature, which corresponds to a ^{85}Rb atomic number density of 2×10^{13} atoms/cm^3. The probe pulses are highly attenuated down to the single-photon level with neutral density filters before being sent into the rubidium cell. The average pho-

ton number per pulse is determined by the measured peak power in the range of pW and a pulse width of 587 ns. The output pulses are measured by off-the-shelf photodetectors from Thorlabs (PDB450A). To observe the signals with high vertical resolution, we used a 12-bit analog-to-digital converter oscilloscope (Teledyne Lecroy HD 4096). To observe the signals with high horizontal resolution, we used a high bandwidth (2.5GHz) oscilloscope (Tektronix 7254C). Error bars shown in the paper represent one standard deviation, combined statistical and systematic uncertainties.

Acknowledgments

We gratefully acknowledge discussions with Ron Folman, Paul Lett, Alberto Marino, Marco Genovese, Daniel Gauthier, Saijun Wu and William Phillips. This work is supported by the National Basic Research Program of China (973 Program grant No. 2011CB921604), National Natural Science Foundation of China under Grants Nos. 11474095, 11274118, 11234003, 11129402, 91436211, 11374104 and 10974057, the Fundamental Research Funds for the Central Universities, the SRFDP (20130076110011), the Program for Professor of Special Appointment (Eastern Scholar) at Shanghai Institutions of Higher Learning, the Program for New Century Excellent Talents in University (NCET-10-0383), the Shu Guang project supported by Shanghai Municipal Education Commission and Shanghai Education Development Foundation (11SG26), the Shanghai Pujiang Program under Grant No. 09PJ1404400, the Scientific Research Foundation of the Returned Overseas Chinese Scholars, State Education Ministry, and Program of State Key Laboratory of Advanced Optical Communication Systems and Networks (2016GZKF0JT003).

Contributions

All authors contributed to all aspects of this work.

Competing financial interests

The authors declare no competing financial interests.

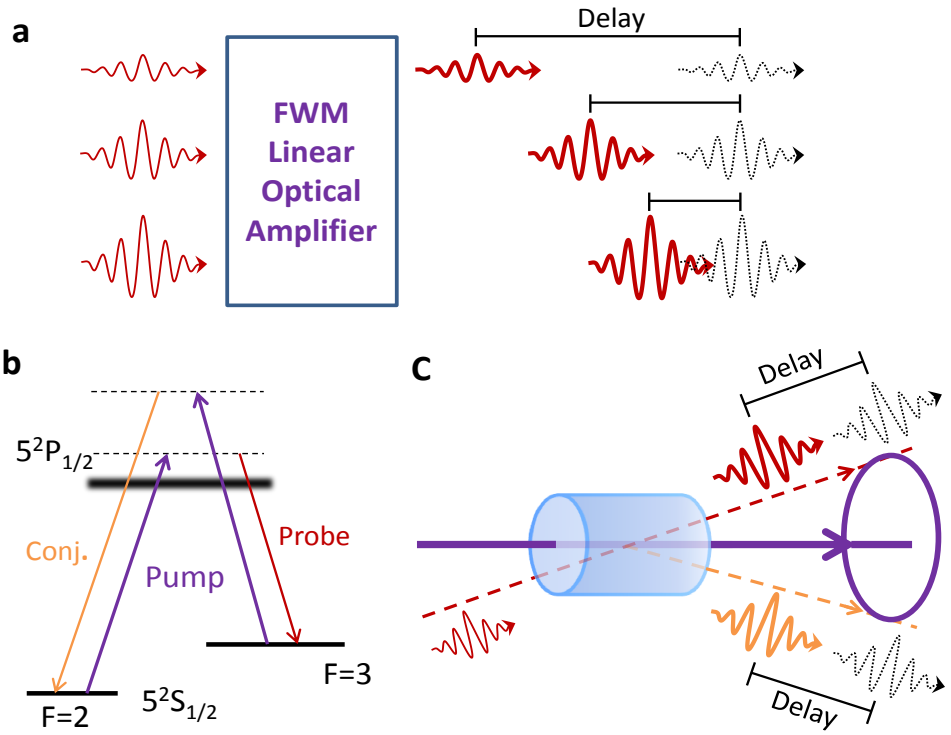

FIG. 1: **Experimental scheme. (a)** The transition time, which is indicated by the group-velocity delay time, is observed to be nonlinearly decayed with the increased input at microscopic level. **(b)** Atomic energy levels of the D1 transition of Rb^{85} involved in the four-wave mixing (FWM) process based on the double-lambda configuration. FWM light fields can be coupled through the atomic coherence between the two ground states, which reduces the resonant losses and increases the relevant nonlinearity. Combined with the large detuning, resonant absorption and spontaneous emission are suppressed. With a strong, non-depleted pump light beam, the system behaves like an optical linear amplifier for input photons. **(c)** The geometry of the experiment. The amplifier provides a large optical gain of 10^7 to amplify the input single-photon level optical signal to the macroscopic level, and to generate a conjugate beam on the opposite side, as well as the resulting slow-light effects.

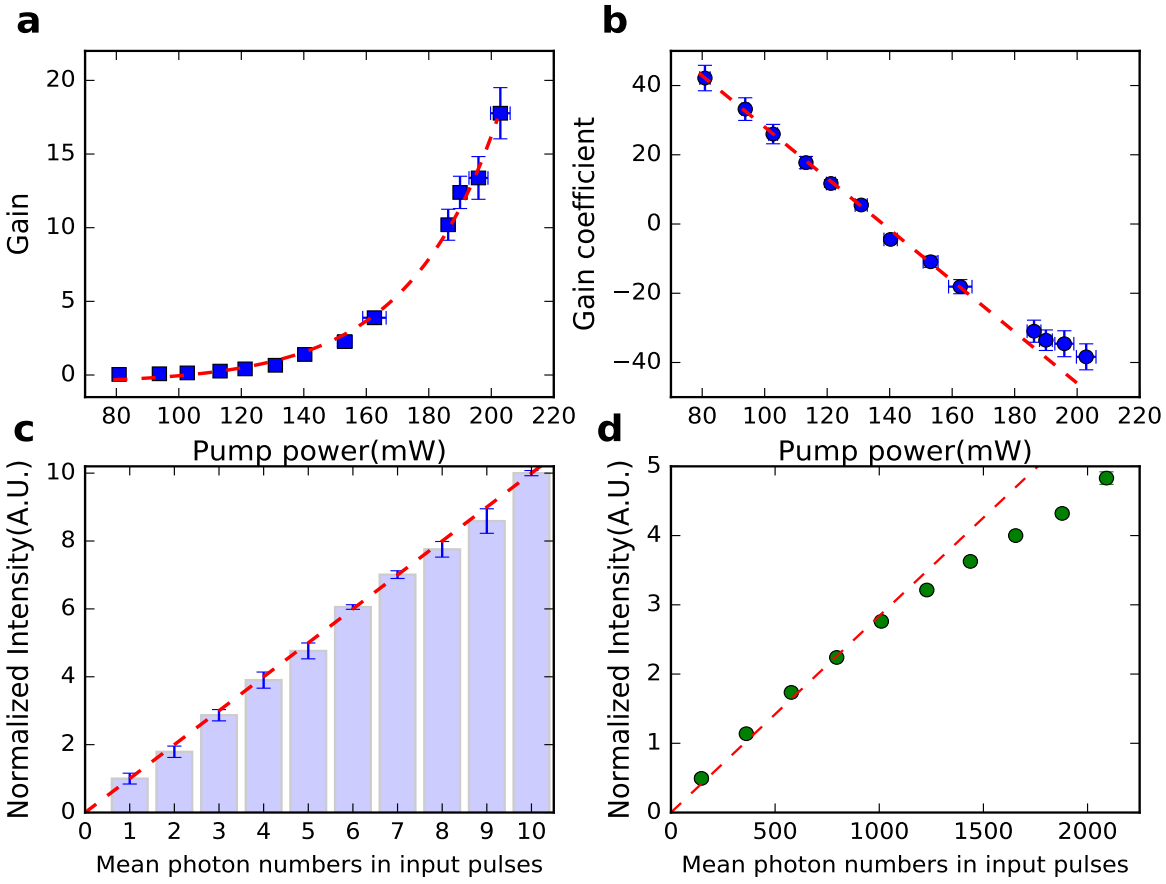

FIG. 2: **Gain properties of the linear optical amplifier. (a)** Gain versus pump power. The gain is exponentially (guide to eye, the red dashed curve) increasing with the pump power. **(b)** The gain coefficient versus pump power. It can be seen that the gain coefficient is linearly (guide to eye, the red dashed curve) tunable in a large range depending on the pump power. **(c)** The output amplitude of the conjugate mode versus the average photon numbers in the input pulses. The red line is linear with a slope of one, and is used as a guide for the eye. To get the significant signal to noise ratios, the plots displayed have been averaged by 10^5 times for the lowest plot and 10^4 times for the highest plot. **(d)** The large scale of dynamic range of conjugate versus mean photon numbers in input pulses. The linearity (guide to eye, the red dashed curve) is preserved up to ∼1000 averaged seed photons. Error bars represent one standard deviation, combined statistical and systematic uncertainties. Error bars in (d) are smaller than the symbols.

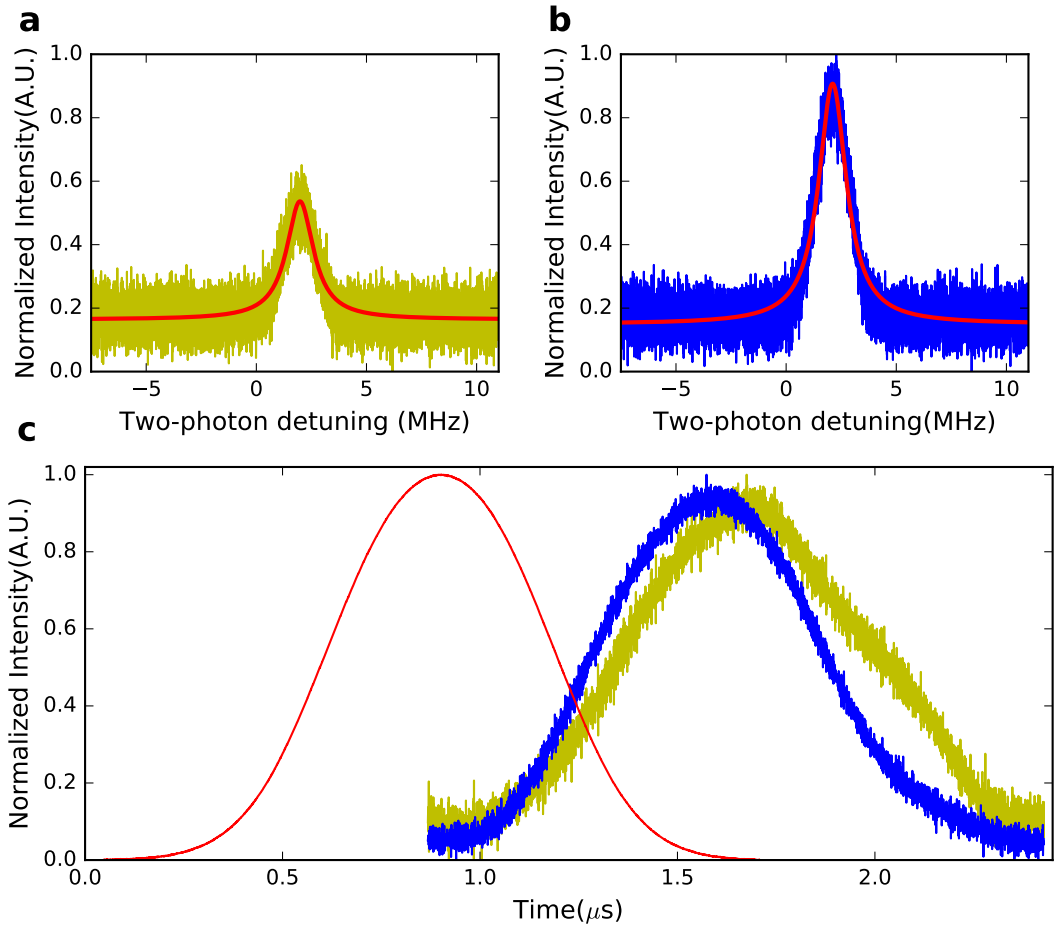

FIG. 3: **Slow light of the output modes. (a)** and **(b)** The gain profiles of probe and conjugate versus two-photon detuning when seeded with a 1pW continuous-wave probe beam. Each profile (a and b) is fitted by a Lorentzian function, indicating the much narrower bandwidths around 1.5 MHz than the natural bandwidth of Rb^{85}, 5.75 MHz. The maximum gain corresponding to an offset is due to the light shift of the pump beam. The output probe beam is weaker than the conjugate due to the Doppler-broadened absorption in its vicinity, which also leads to more distorted output probe pulses. **(c)** The delays of the output probe and conjugate pulses at two different frequencies when injected with probe pulse containing 0.7 photons on average. The delay times for the probe and conjugate pulses are 672ns (yellow curve) and 592ns (blue curve), with fractional delay of 1.14 and 1.01, respectively. The plots are averaged for 10^4 times. The red curve is the reference pulse taken with propagation at the vacuum speed of light. All the plots are superposed on a constant background from the unseeded conical emission and normalized to facilitate comparison of input and output pulse shapes.

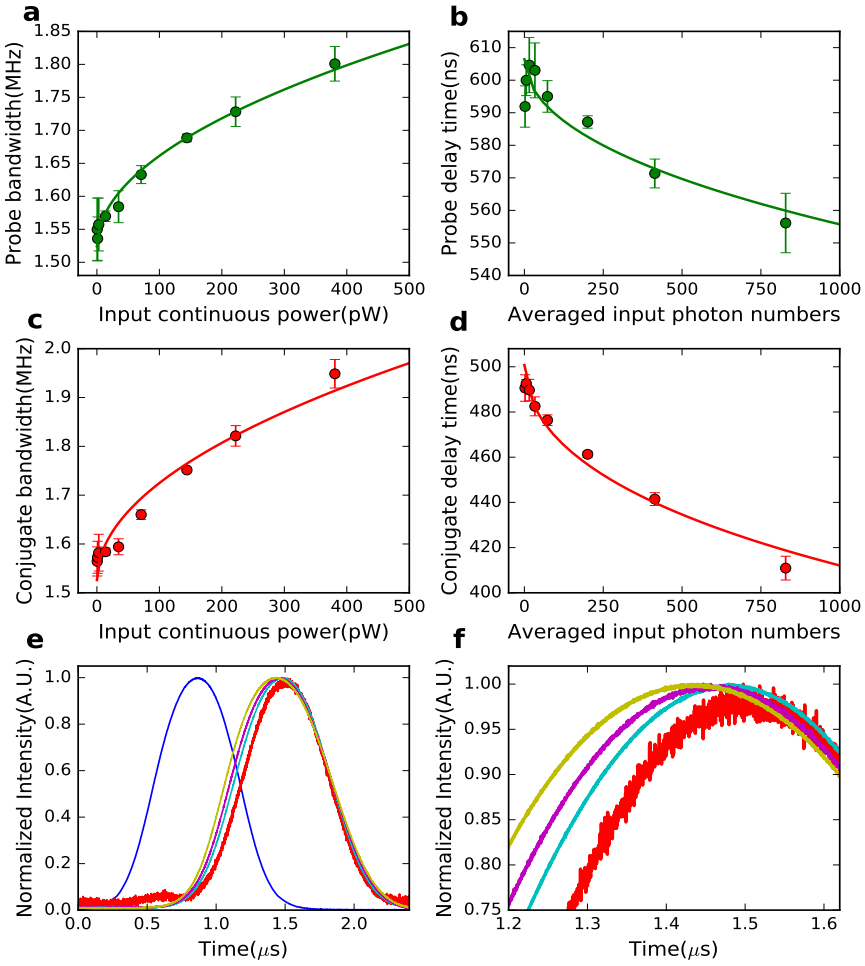

FIG. 4: **Dispersion-delay time matching.** **(a)** and **(c)** The bandwidths of the probe and conjugate gain profiles versus input continuous power. **(b)** and **(d)** The delay of the conjugate pulses versus averaged input photon numbers. The fits from Eq.(1) are essentially of the form of $s \cdot \sqrt{x} + z$ for ((a) and (c)), and $1/(s \cdot \sqrt{x} + z)$ for ((b) and (d)), in which s characterizes the dispersion's sensitivity on the input power and z is the off-set determined by the system. For conjugate, s_c and s_d are 1.988 $\pm 0.39 \times 10^5 GHz/\sqrt{pW}$ and 2.154 $\pm 0.33 \times 10^5 GHz/\sqrt{pW}$. For probe, s_a and s_b are 1.373 $\pm 0.144 \times 10^5 GHz/\sqrt{pW}$ and 0.729 $\pm 0.292 \times 10^5 GHz/\sqrt{pW}$. The conjugate has stronger sensitivity and better bandwidth-delay time matching due to less absorption. **(e)-(f)** Typical delayed pulses and highlighted peak parts in the conjugate mode for different averaged input photon numbers of 413 (yellow), 200 (purple), 73 (green), 2 (red), and reference pulse (blue).

[1] Arndt, M., Nairz, O., Vos-Andreae, J., Keller, C., van der Zouw, G. and Zeilinger, A. Wave-particle duality of C_{60} molecules. *Nature* **401,** 680 (1999).

[2] Friedman, J. R., Patel, V., Chen, W. , Tolpygo, S. K. and Lukens, J. E. Quantum superposition of distinct macroscopic states. *Nature* **406,** 43 (2000).

[3] Julsgaard, B., Kozhekin, A. and Polzik, E. S., Experimental long-lived entanglement of two macroscopic objects, Nature **413**, 400 (2001).

[4] O′Connell, A. D., et al. Quantum ground state and single-phonon control of a mechanical resonator. *Nature* **464,** 697 (2010).

[5] Lamas-Linares, A., Howell, J. C. and Bouwmeester, D. Stimulatedemissionof polarization-entangled photons. *Nature* **412,** 887 (2001).

[6] Lamas-Linares, A., Simon, C., Howell, J. C. and Bouwmeester, D., Experimental Quantum Cloning of Single Photons, *Science* **296,** 712 (2002).

[7] Simon, C. and Bouwmeester, D. Theory of an Entanglement Laser. *Phys. Rev. Lett.* **91,** 053601 (2003).

[8] F. De, Martini, Sciarrino, F. and Vitelli, C. Entanglement Test on a Microscopic-Macroscopic System. *Phys. Rev. Lett.* **100,** 1253601 (2008).

[9] Raeisi, S., Tittel, W. and Simon, C. Proposal for Inverting the Quantum Cloning of Photons. *Phys. Rev. Lett.* **108,** 120404 (2012).

[10] Fickler, R., et al. Quantum Entanglement of High Angular Momenta, *Science* **338,** 640 (2012).

[11] Sekatski, P., et al. Proposal for exploring macroscopic entanglement with a single photon and coherent states. *Phys. Rev. A* **86,** 060301(R) (2012).

[12] Ghobadi, R., Lvovsky, A. and Simon, C. Creating and Detecting Micro-Macro Photon-Number Entanglement by Amplifying and Deamplifying a Single-Photon Entangled State. *Phys. Rev. Lett* **110,** 170406 (2013).

[13] Sekatski, P., Aspelmeyer, M. and Sangouard, N. Macroscopic Optomechanics from Displaced Single-Photon Entanglement. *Phys. Rev. Lett.* **112,** 080502 (2014).

[14] Ghobadi, R., Kumar, S., Pepper, B., Bouwmeester, D., Lvovsky, A. I. and Simon, C. Optomechanical Micro-Macro Entanglement. *Phys. Rev. Lett.* **110,** 170406 (2014).

[15] Vered, R. Z., Shaked, Y., Ben-Or, Y., Rosenbluh, M. and Pe'er, A. Classical-to-Quantum

Transition with Broadband Four-Wave Mixing. *Phys. Rev. Lett.* **114,** 063902 (2015).

[16] Ou, Z. Y., Pereira, S. F., Kimble, H. J. and Peng, K. C. Realization of the Einstein- Podolsky-Rosen paradox for continuous variables. *Phys. Rev. Lett.* **68,** 3663 (1992).

[17] Howell, J. C., Bennink, R. S., Bentley, S. J. and Boyd, R.W. Realization of the Einstein-Podolsky-Rosen Paradox Using Momentum-and Position-Entangled Photons from Spontaneous Parametric Down Conversion. *Phys. Rev. Lett.* **92,** 210403 (2004).

[18] Silberhorn, C., Lam, P. K., Weiss, O., Koenig, F., Korolkova, N. and Leuchs, G. Generation of Continuous Variable Einstein-Podolsky-Rosen Entanglement via the Kerr Nonlinearity in an Optical Fiber. *Phys. Rev. Lett.* **86,** 4267(2001).

[19] Harris, S. E. Lasers without inversion: interference of lifetime-broadened resonances. *Phys. Rev. Lett.* **62,** 1033 (1989).

[20] Boller, K. J., Imamoglu, A. and Harris, S. E. Observation of electromagnetically induced transparency. *Phys. Rev. Lett.* **66,** 2593 (1991).

[21] Fleischhauer, M., Imamoglu, A. and Marangos, J. P. Electromagnetically induced transparency: Optics in coherent media. *Rev. Mod. Phys.* **77,** 633 (2005).

[22] Kash, M. K., et al. Ultraslow group velocity and enhanced nonlinear optical effects in a coherently driven hot atomic gas. *Phys. Rev. Lett.* **82,** 5229 (1999).

[23] Lukin, M. D. Trapping and manipulating photon states in atomic ensembles. *Rev. Mod. Phys.* **75,** 457 (2003).

[24] Boyer, V., McCormick, C. F., Arimondo, E. and Lett, P. D. Ultraslow propagation of matched pulses by four-wave mixing in an atomic vapor. *Phys. Rev. Lett.* **99,** 143601 (2007).

[25] Camacho, R. M., Vudyasetu, P. K. and Howell, J. C. Four-wave-mixing stopped light in hot atomic rubidium vapour. *Nat. Photon.* **3,** 103-106 (2009).

[26] Hammerer, K., Sorensen, A. S. and Polzik, E. S. Quantum interface between light and atomic ensembles. *Rev. Mod. Phys.* **82,** 1041 (2010).

[27] Eisaman, M. D., Andre, A., Massou, F., Fleischhauer, M., Zibrov, A. S. and Lukin, M. D. Electromagnetically induced transparency with tunable single-photon pulses. *Nature* **438,** 837 (2005).

[28] Akopian, N., Wang, L., Rastelli, A., Schmidt, O. G. and Zwiller, V. Hybrid semiconductor-atomic interface: slowing down single photons from a quantum dot. *Nature Photonics* **5,** 230 (2011).

[29] Hockel, D. and Benson, O. Electromagnetically Induced Transparency in Cesium Vapor with Probe Pulses on the Single-Photon Level. *Phys. Rev. Lett.* **105,** 153605 (2010).

[30] Dressel, J., Rajeev, S. G., Howell, J. C., and Jordan, A. N. Gravitational redshift and deflection of slow light. *Phys. Rev. A* **79,** 013834 (2009).

[31] Kumar, N. Deflection of ultra-slow light by the Earth's gravity on laboratory length scale. *Europhys. Lett.* **82,** 60002 (2008).

[32] Bekenstein, R., Schley, R., Mutzafi, M., Rotschild C. and Segev, M. Optical simulations of gravitational effects in the NewtonSchrödinger system *Nat. Phys.* **11,** 872 (2015).

[33] Liao, W.-T. and Ahrens, S. Gravitational and relativistic deflection of X-ray superradiance *Nat. Photon.* **9,** 169 (2015).

[34] McCormick, C. F., Marino, A. M., Boyer, V. and Lett, P. D. Strong low-frequency quantum correlations from a four-wave-mixing amplifier. *Phys. Rev. A* **78,** 043816 (2008).

[35] Marino, A. M., Pooser, R. C., Boyer, V. and Lett, P. D. Tunable delay of EinsteinPodolsky-Rosen entanglement. *Nature* **457,** 859 (2009).

[36] Concannon, H. M., Brown, W. J., Gardner, J. R. and Gauthier, D. J. Observation of large continuous-wave two-photon optical amplification. *Phys. Rev. A* **56,** 1519 (1997).

[37] Dawes, A. M. C., Illing, L., Clark, S. M. and Gauthier, D. J. All-optical switching in rubidium vapor. *Science* **308,** 672-674 (2005).

[38] Supplementary materials are online.

[39] Turnbull, M. T., Petrov, P. G., Embrey, C. S., Marino, A. M. and Boyer, V. Role of phase-matching condition in nondegeneratre four-wave mixing in hot vapors for the generation of squeezed states of light. *Phys. Rev. A* **88,** 033845 (2013).

[40] van der Wal, C. H., Eisaman, M. D., Andre, A., Walsworth, R. L., Phillips, D. F., Zibrov, A. S., Lukin, M. D. Atomic Memory for Correlated Photon States. *Science* **301,** 196(2003).

[41] Lukin, M. D., Hemmer, P. R. and Scully, M. O. Resonant nonlinear optics in phase-coherent media. *Adv. At. Mol. Opt. Phys.* **42,** 347 (2000).

[42] Phillips, N. B., Gorshkov, A. V. and Novikova, I. Slow light propagation and amplification via electromagnetically induced transparency and four-wave mixing in an optically dense atomic vapor. *Journal of Modern Optics* **56,** 1917 (2009).

[43] Boyd, R. W. and Gauthier, D. J. Slow and fast light. *Progress in Optics*, E. Wolf, Ed. (Elsevier, Amsterdam, 2002), Vol. 43.

[44] Boyd, R. W. *Nonlinear optics*, 3rd ed. (Academic, 2008).

[45] MacRae, A., Brannan, T., Achal, R. and Lvovsky, A. I. Tomography of a High-Purity Narrowband Photon from a Transient Atomic Collective Excitation. *Phys. Rev. Lett* **109**, 033601 (2012).

[46] Bassi, A., Lochan., K., Satin, S., Singh, T. P. and Ulbricht, H. Models of wave-function collapse, underlying theories, and experimental tests. *Rev. Mod. Phys.* **85,** 471 (2013).

[47] Margalit, Y., Zhou, Z., Machluf, S., Rohrlich, D., Japha, Y. and Folman, R. A self-interfering clock as a " which path" witness, *Science* **349**, 1205 (2015).

Supplementary material for

Characterizing micro-macro transitions with slow light

S1. Doppler broadened absorption, conical emission and spectra

The Doppler-broadened spectra of the rubidium cell are shown in Fig.S1. The origin corresponds to the $5S_{1/2}$ (F=2) to $5P_{1/2}$ transition of ^{85}Rb D1 line. We set the pump frequency around 1.25 GHz blue-detuned from the $5S_{1/2}$ (F=2) to $5P_{1/2}$ transition to avoid the Doppler-broadened absorption. When the pump power is 300mW, the observed conical emission with a pattern of ring is shown in Fig.S2a. The ring has a half-angle cone of roughly 8mrad. The conical emission angle is affected by the system parameters, such as cell temperature and pump's one-photon detuning frequency [39].

After filtering out the residual pump power with a Glan-Taylor polarizer after the cell, the ring contains photons at the probe and conjugate frequencies with frequency difference of ∼6GHz (Fig.S2c), considering that the ground-state splitting of ^{85}Rb is 3.035 GHz. The majority of the generated photons are at the conjugate frequency due to the strong absorption at the probe frequency with the present rubidium system (Fig.S1). When the system is injected with 1pW continuous input power, the observed pattern is shown in Fig. S2b. The probe beam is weaker due to the additional Doppler-broadened absorption.

S2. Group-velocity delay times versus pump power

In the present experiment, the group-velocity delay times can be tuned by changing the pump powers. Due to power broadening, the gain profile's bandwidth is proportional to the pump intensity (Fig.S3 inset), which modifies the dispersion to be less steep as the pump power increases, resulting in less group-velocity delay. Figure S3 shows the output pulse delay's dependence on the pump power when the input probe pulses contain 3.8 photons on average. The measurement in Fig.S3 shows that the group delay can be tuned by changing the pump power. The relative delay between the conjugate and probe pulses is a fundamental feature of this scheme [24, 40, 41].

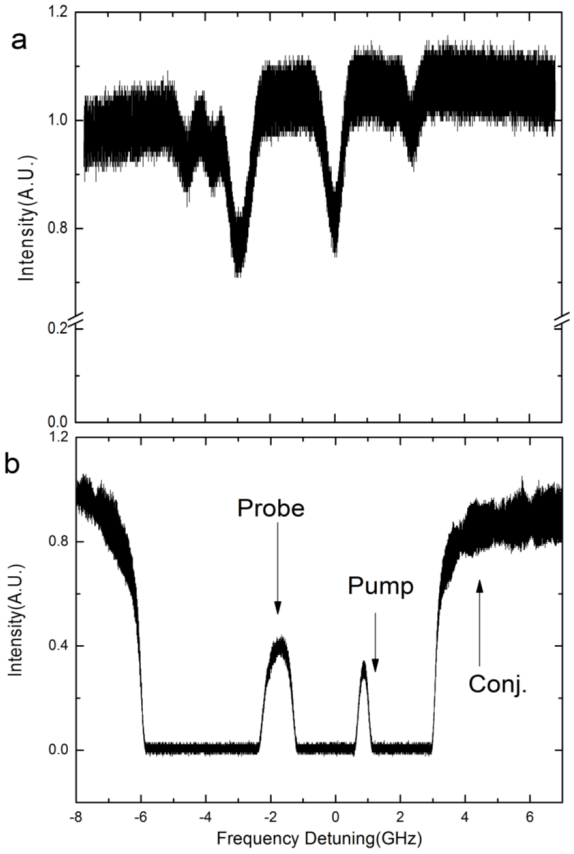

FIG. S1: Doppler broadened absorption profiles of the rubidium cell at the room temperature **(a)**, and at the working temperature of 130°C **(b)**. The frequencies of probe, pump and conjugate are indicated by the arrows.

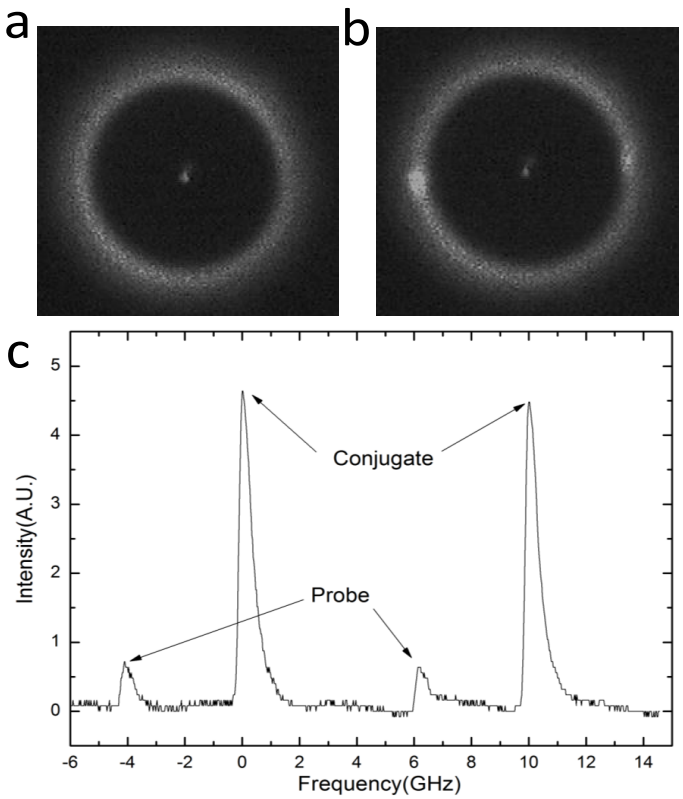

FIG. S2: FWM output pattern observed in the far field for the case without input **(a)**, and with 1pW continuous input **(b)**. The bright spots are the amplified probe beam (right spot) and generated conjugate beam (left spot), respectively. **(c)** The spectrum of conical emission photons is measured by a Fabry-Perot cavity with a free spectral range of 10GHz. The displayed figure contains results of two scanning cycles.

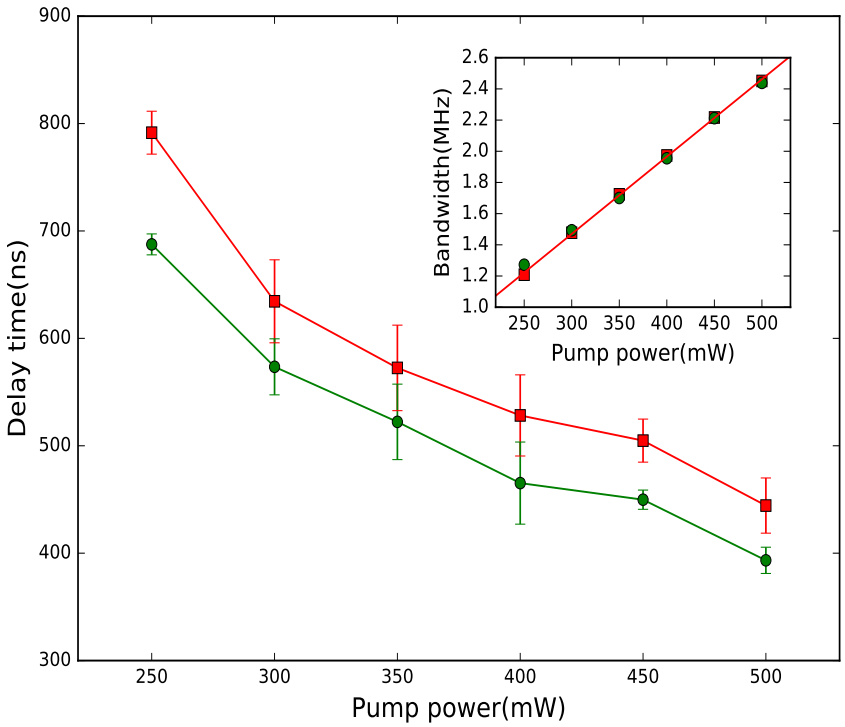

FIG. S3: The delays of the output probe pulses (red squares) and the output conjugate pulses (green circles) versus pump power are shown. The upper right inset shows the gain profile's bandwidth of the probe (red squares) and conjugate (green circles) versus pump power. Due to a power broadening effect, the bandwidth is proportional to the pump power, and thus shows good agreement with a linear fit. This bandwidth broadening makes the corresponding dispersion less-steep and leads to less delay. Error bars represent one standard deviation, combined statistical and systematic uncertainties. The error bars in the inset figure are smaller than the symbols' size.